

## Radioactive Airborne Species Formed in the Air in High Energy Accelerator Tunnels

K. Kondo\*

High Energy Accelerator Research Organization (KEK) 1-1 Oho, Tsukuba, Ibaraki 305-0801, Japan

Received: March 31, 2006

The particle size distributions of radioactive nuclides formed in accelerator beam line tunnels were measured by using a diffusion battery and were found to be log-normal with a geometric mean radius of about 28 nm. The radioactive aerosol formation was well explained by a simple physical adsorption of radioactive nuclides to the ambient non-radioactive aerosols. The fractions of aerosol and gaseous components were measured for individual nuclides formed in the air of a high-energy accelerator tunnel. The formation of these  $^{11}\text{C}$  and  $^{13}\text{N}$  species was explained by their hot-atom reactions and subsequent chemical reactions.

### 1. Introduction

High-power and high-energy proton accelerators have been proposed for basic scientific research in several countries, and some of them are under construction. In Japan, the high intensity proton accelerator (J-PARC), consisting of a 200-MeV Linac as well as 3-GeV and 50-GeV synchrotrons, of which the maximum beam power is about 1MW, is to be completed at the end of 2007. This accelerator was designed for a broad range of frontier sciences using pulsed-intense neutrons from the 3-GeV synchrotron and neutrino and K beam from the 50-GeV synchrotron.<sup>1</sup>

At these accelerators, the air in the beam line tunnel is exposed to extremely high radiation fields during machine operation, where primary and secondary high-energy particles coexist. A number of radioactive nuclides are abundantly produced in the air, mainly through a variety of nuclear reactions between these high-energy particles and the elements of air. These nuclides generally behave as hot atoms with high kinetic energies and charges, and after completion of hot-atom reactions, part of them form radioactive aerosols and others are present in a gaseous form. Studying the physico-chemical properties of these radioactive airborne species is an interesting subject from radiochemical standpoint.

Moreover, airborne radioactive nuclides become a source of external and internal exposures for workers when entering the accelerator tunnels after a shutdown of machine operation. To evaluate internal doses from radioactive nuclides induced in the air, information on their particle sizes and chemical forms is indispensable. However, thus far, there is little information available on these physical and chemical properties of airborne radioactive nuclides formed in the air in accelerator beam-line tunnels.

An extensive study has been conducted on the physico-chemical properties of airborne radioactive nuclides. In this paper, a review is given of recent results.

### 2. Experimental Procedure

**(a) Measurement of the particle size distribution of radioactive aerosols.** The air in the proton beam line of the KEK (High Energy Accelerator Research Organization) 12-GeV synchrotron was sampled from an open space between the D1 magnet and the iron beam dump. Figure 1(a) shows a cross-

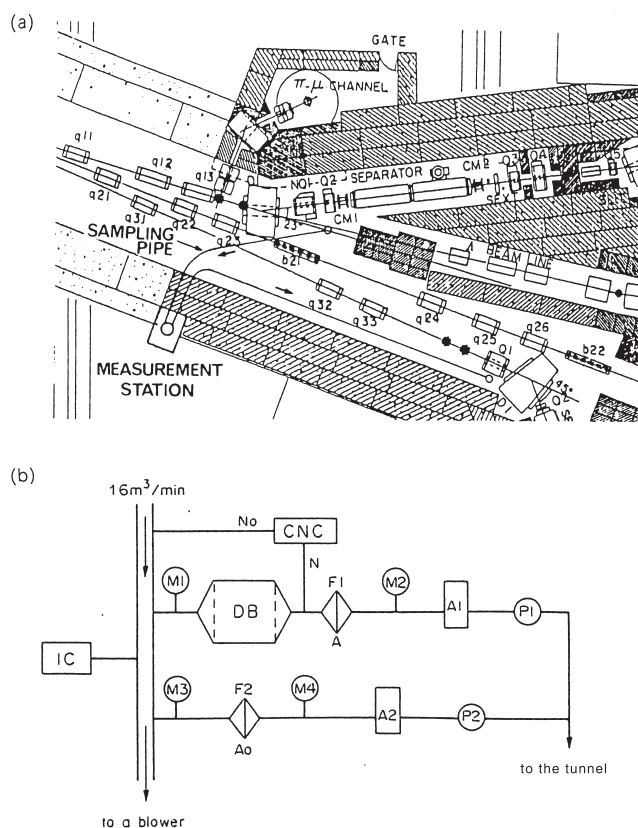


**Figure 1.** (a) KEK-slow extracted proton beam line (EP2) and (b) schematic diagram of measurement. CNC: condensation nuclei counter, DB: parallel plate diffusion battery, F1,F2: filter, A1,A2: flow-meter, P1,P2: pump, M1,M2: mercury manometer, IC: ionization chamber, A,A<sub>0</sub>: radioactivities collected on the filter, N,N<sub>0</sub>: aerosol number.

sectional view around the sample position. The sample inlet is about 50 cm above the beam axis and ~3.5 m downstream from the target, which is used for the production of secondary particles, such as K,  $\pi$ -mesons, and electrons. Figure 1(b) shows a schematic diagram of measurements at a measurement station that was placed outside of concrete shield. The details of the sampling conditions of the air are described in References 2–5. For determining the size distribution of the radioactive aerosols, a diffusion method was applied by using a diffusion battery with parallel-side channels (PPDB).

The diffusion losses of aerosol particles from an aerosol

\*Corresponding author. E-mail: Kenjiro.Kondo@kek.jp

undergoing a laminar flow through the channels of a PPDB depend on the diffusion coefficient of the particles, the mean linear rate of the aerosol flow, and the dimensions of the channel. For mono-dispersed aerosols, the penetration fraction ( $P$ ) with this type of battery is given by the DeMarcus' equation,<sup>6</sup>

$$P = \frac{n}{n_0} = 0.9149 \exp(-3.77v) + 0.0592 \exp(-44.6v) + 0.026 \exp(-302v). \quad (1)$$

Here  $n$  and  $n_0$  are the particle concentrations at the exit and entrance of the battery, respectively, and  $v$  is an experimental parameter. The diffusion coefficient ( $D$ ) and  $v$  are defined by the following equations:

$$v = \frac{NDbt}{tQ}, \quad (2)$$

$$D = \frac{kT}{6\pi\eta r} \left[ 1 + A \frac{L}{r} + C \frac{L}{r} \exp\left(-\frac{Br}{L}\right) \right], \quad (3)$$

where  $N$  is the channel number of a diffusion battery,  $r$  the aerosol radius,  $t$  the half width between the plates,  $b$  the height of the battery,  $l$  the length of the battery,  $Q$  the flow rate,  $k$  Boltzman's constant ( $1.38 \times 10^{-16}$  erg  $K^{-1}$ ),  $T$  the temperature (K),  $L$  the mean-free path of air molecules ( $0.653 \times 10^{-5}$  cm) and  $\eta$  the viscosity of the air ( $1.83 \times 10^{-4}$  dyne  $cm^{-2}$  at 296 K and 101.3 kPa).  $A$ ,  $B$ , and  $C$  are coefficients for Cunningham's correction ( $A = 1.246$ ,  $B = 0.87$ , and  $C = 0.42$ ). The dimensions of the PPDB used in the present work were  $N = 20$ ,  $t = 0.05$  cm,  $b = 20$  cm, and  $l = 57$  cm.

Generally aerosols are polydisperse and of a log-normal distribution. The following generalized DeMarcus' equation is assumed for aerosols with a log-normal distribution of particle sizes<sup>7</sup>:

$$P = \frac{0.9149}{\sqrt{2\pi} \log \sigma_g} \int_{-\infty}^{+\infty} \exp(-3.77v) \exp\left[-\frac{(\log r - \log r_g)^2}{2 \log^2 \sigma_g}\right] d \log r + \frac{0.0592}{\sqrt{2\pi} \log \sigma_g} \int_{-\infty}^{+\infty} \exp(-44.66v) \exp\left[-\frac{(\log r - \log r_g)^2}{2 \log^2 \sigma_g}\right] d \log r, \quad (4)$$

where  $r_g$  and  $\sigma_g$  are the mean geometric radii and the standard geometric deviations, respectively. The third term in eq 1 can be neglected in view of its smallness.

In the present work,  $n/n_0$  can be replaced by the ratio of the radioactivity collected on the filter ( $A$ ) through the PPDB to the total radioactivity ( $A_0$ ). The radioactivities,  $A$  and  $A_0$ , were collected at the same time, as Figure 1 shows. The relation of  $P$  vs  $Q$  was obtained experimentally, and then the  $r_g$  and  $\sigma_g$  values were evaluated from curve fitting method using a least-squares-fitting computer code (SALS).<sup>8</sup>

**(b) Radioactive aerosol formation using Ar gas containing dioctyl phthalate aerosols.** In order to investigate more precisely the formation mechanism of radioactive aerosols under well defined experimental conditions, argon gas containing dioctyl phthalate (DOP) aerosols was irradiated 65 MeV quasi-monoenergetic neutrons produced from the  ${}^7\text{Li}(p, n)$  reaction by bombarding a 5.2 mm thick  ${}^7\text{Li}$ -target with 68 MeV protons from an AVF cyclotron. The experiment was carried out at Takasaki Ion Accelerator for Advanced Radiation Application (TIARA) of the Japan Atomic Energy Research Institute. Figures 2(a) and 2(b) show a schematic view of the monoenergetic neutron source and a block diagram of the experimental setup. All charged particles were swept out by a clearing magnet, and the chamber was irradiated by pure monoenergetic neutrons. The argon gas served as a target for the production of radioactive nuclides as well as a gaseous medium for suspending the DOP aerosols. As predominant radioactive nuclides,  ${}^{38}\text{Cl}$  ( $T_{1/2} = 37.2$  min) and  ${}^{39}\text{Cl}$  ( $T_{1/2} = 55.6$  min) are produced through the  $(n, 2np)$  and  $(n, np)$  reactions of  ${}^{40}\text{Ar}$ . High-purity Ar gas was flowed into the irradiation chamber at a flow rate of 20 L/min for 5 min. Then, the DOP aerosols were generated from liquid DOP using an atomizer (Model

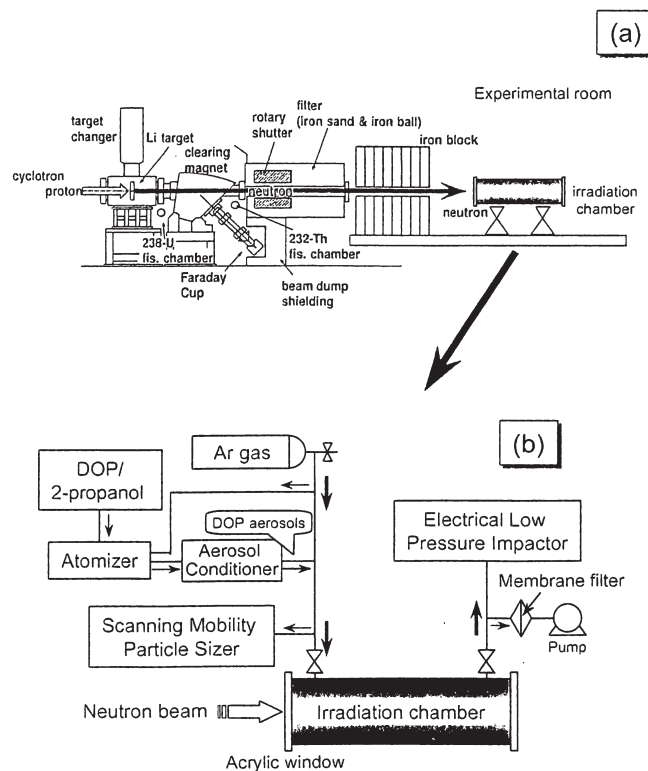


**Figure 2.** (a) Schematic view of the mono-energetic neutron source facility at TIARA. (b) Block diagram of the experimental setup.

3075, TSI Inc.) and the thus-obtained poly-disperse DOP aerosols were evaporated and condensed in the aerosol conditioner (Model 3072, TSI Inc.). The volume fraction of DOP in 2-propanol was 10% and the flow rate of argon was 1 L/min. The size distribution of the DOP was measured with a scanning mobility particle sizer (SMPS Model 3936L22, TSI Inc.) consisting of an electrostatic classifier and a condensation particle counter, which can measure the size distribution of aerosols in the particle diameter range from 0.01 to 1  $\mu\text{m}$  over a wide range of concentrations (from 2 to  $10^8$  particles/ $\text{cm}^3$ ). After confirming the particle size distribution, the aerosol suspended in argon was introduced into the argon-filled irradiation chamber for 5 min, and then the inlet and outlet of the chamber were closed. The concentration of the DOP aerosols in the chamber was on the order of  $10^4$  particles/ $\text{cm}^3$ . The prepared sample-gas was irradiated with 65 MeV quasi-monoenergetic neutrons of  $2.3 \times 10^4 \text{ cm}^{-2} \text{ s}^{-1}$  for 60–120 min. After irradiation, the sample gas was collected with a membrane filter at a flow rate of 20 L/min. The size distribution of the aerosols was measured using an electrical low-pressure impactor (Model ELPI-2000, Dekati.). For the activity-weighted size distribution, the collection substrates of the impactor stages were removed after sampling and their radioactivities were measured using a gas-flow counter.

**(c) Measurement of chemical forms of  ${}^{11}\text{C}$  and  ${}^{13}\text{N}$  airborne species.** Measurements of  ${}^{11}\text{C}$  and  ${}^{13}\text{N}$  chemical species were carried out by using a chamber consisting of a cylindrical and trapezoidal vessels made of aluminum having a volume of 0.67  $\text{m}^3$  at the slow extracted proton beam line (EP-2) of the KEK 12-GeV synchrotron. A measurement station consisting gas-sampling and analyzing systems was placed in an area outside of the accelerator shielding. Atmospheric air free from aerosols or high-purity mixed gas ( $\text{N}_2$  80% and  $\text{O}_2$  20%) from a gas cylinder was continuously supplied into the irradiation chamber. The details of the sampling conditions of the air are described in References 9–12.

Possible species of  ${}^{11}\text{C}$  in the irradiated air would be  ${}^{11}\text{C}$ ,  ${}^{11}\text{CO}_2$ ,  ${}^{11}\text{C}$ -hydrocarbons, and  $\text{H}^{11}\text{CN}$ . A measurement of the concentration of these species was carried out by a sampling

method using alkaline traps and a cold trap. After removing the radioactive aerosols with the membrane filter at a flow rate of 0.3 L/min,  $^{11}\text{C}$  was collected in the first KOH trap and  $^{11}\text{CO}$  was collected in the second KOH trap after being oxidized to  $^{11}\text{CO}_2$  by the hopcalite. The radioactivity in each trap was measured by  $\gamma$ -ray spectrometry. The total  $^{11}\text{C}$  activity was obtained by a system consisting of a membrane filter, a Pd catalyst and a KOH trap. The Pd catalyst maintained at  $550^\circ\text{C}$  oxidized both  $^{11}\text{CO}$  and  $^{11}\text{C}$ -hydrocarbons to  $^{11}\text{CO}_2$ . The collection of  $\text{H}^{11}\text{CN}$  was carried out by the cold trap kept at  $-25^\circ\text{C}$ , in which  $\text{H}^{11}\text{CN}$  could be collected. The sampled air was also analysed with a radio-gaschromatograph.

A new filter technique was developed for the analysis of individual chemical species of  $^{13}\text{N}$ . The filter packs for collecting  $^{13}\text{NO}_2$  and  $^{13}\text{NO}$  consisted of  $\text{Na}_2\text{CO}_3$ -,  $\text{NiO}$ -, and  $\text{Co}_2\text{O}_3$ -impregnated filter arranged in series.<sup>10</sup> After removing radioactive aerosols by passing through a Teflon filter,  $\text{H}^{13}\text{NO}_2$  and  $\text{H}^{13}\text{NO}_3$  were collected by a  $\text{Na}_2\text{CO}_3$ -impregnated filter.  $^{13}\text{NO}_2$  and  $^{13}\text{NO}$  were separately collected on the  $\text{NiO}$ -, and  $\text{Co}_2\text{O}_3$ -impregnated filters, respectively. Further, selective collection systems for  $\text{H}^{13}\text{NO}_2$  and  $\text{H}^{13}\text{NO}_3$  consist of two sets of assemblies. One was for the total  $\text{H}^{13}\text{NO}_3$  and  $\text{H}^{13}\text{NO}_2$ , and the other was for  $\text{H}^{13}\text{NO}_2$  alone.  $\text{H}^{13}\text{NO}_3$  and  $\text{H}^{13}\text{NO}_2$  were selectively stripped from the sample air into a scrubbing solution (0.05M NaOH) as a nitrite and nitrate, respectively. The nitrate was reduced with hydrazine sulfate in the presence of  $\text{Cu(II)}$  to nitrite, which was then reduced to  $^{13}\text{NO}$  with ascorbic acid solution.  $\text{H}^{13}\text{NO}_3$  was determined by the difference between the two measurements.

### 3. Results and Discussion

**(a) Gaseous and aerosol fractions of airborne nuclides.** The typical  $\gamma$ -ray spectrum of radioactivities collected on the filter is shown in Figure 3. The number of radioactive nuclides found in this experiment was relatively small compared to the number of possible radioactive nuclides expected to be produced. This could be explained as follows; (a) their concentrations were too low to detect by  $\gamma$ -ray spectroscopy. (b) Some of the nuclides were pure- $\beta$  emitters. The airborne radioactivity concentrations for individual nuclides changed from one measurement to another depending on the conditions of machine operation, such as the beam intensity and the degree of beam loss. The concentrations for the principal nuclides were  $\sim 7 \times 10^{-1} \text{ Bq/cm}^3$  for  $^{11}\text{C}$ ,  $\sim 1.5 \text{ Bq/cm}^3$  for  $^{15}\text{O}$ ,  $\sim 5.9 \times 10^{-5} \text{ Bq/cm}^3$  for  $^3\text{H}$ ,  $\sim 1.7 \times 10^{-4} \text{ Bq/cm}^3$  for  $^7\text{Be}$ ,  $\sim 9.6 \times 10^{-5} \text{ Bq/cm}^3$  for  $^{24}\text{Na}$ , and  $\sim 5.6 \times 10^{-5} \text{ Bq/cm}^3$  for  $^{38}\text{S}$ .

The aerosol fractions were estimated to be  $\sim 1.9\%$  for  $^{11}\text{C}$  and  $^{13}\text{N}$ ,  $0.5\%$  for  $^{15}\text{O}$ , and  $\sim 0.05\%$  for  $^{18}\text{F}$ . For  $^{38}\text{S}$ ,  $^{38}\text{Cl}$ , and  $^{39}\text{Cl}$ , they were found to have both aerosol and gaseous components from measurements using a NaOH filter paper. The aerosol fractions were  $50\%$  for  $^{38}\text{S}$ ,  $78\%$  for  $^{38}\text{Cl}$ , and  $72\%$  for  $^{39}\text{Cl}$ . In the case of  $^{38}\text{Cl}$ , the genetic relation between  $^{38}\text{S}$  and  $^{38}\text{Cl}$  was taken into account. The radioactive nuclides other than those nuclides were present as  $100\%$  aerosols. A summary of these measurements is given in Table 1. So far, little is known about the fractions of gaseous and aerosol components for the nuclides produced in the air of accelerator tunnels. These results give useful information for estimating internal radiation doses.

**(b) Particle size distribution of radioactive aerosols and mechanisms of radioactive aerosol formation.** Figure 4 shows the relations of  $A/A_0$  vs  $Q$  obtained by using the PPDB for  $^7\text{Be}$ -,  $^{24}\text{Na}$ -, and  $^{38}\text{S}$ -aerosols. Measurements for other radioactive nuclides, except those three nuclides, were not conducted because of their low radioactivities. The experimental errors in the figure are the standard deviations for the counting statistics. The solid lines indicate the best results of the least-squares fitting. Statistical analyses gave the parameters  $r_g$

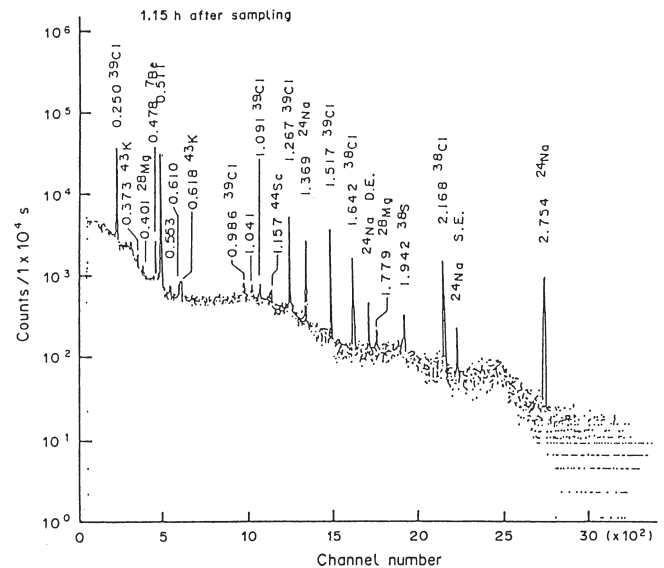


Figure 3. Typical  $\gamma$ -ray spectrum of the radioactivity collected on the filter.

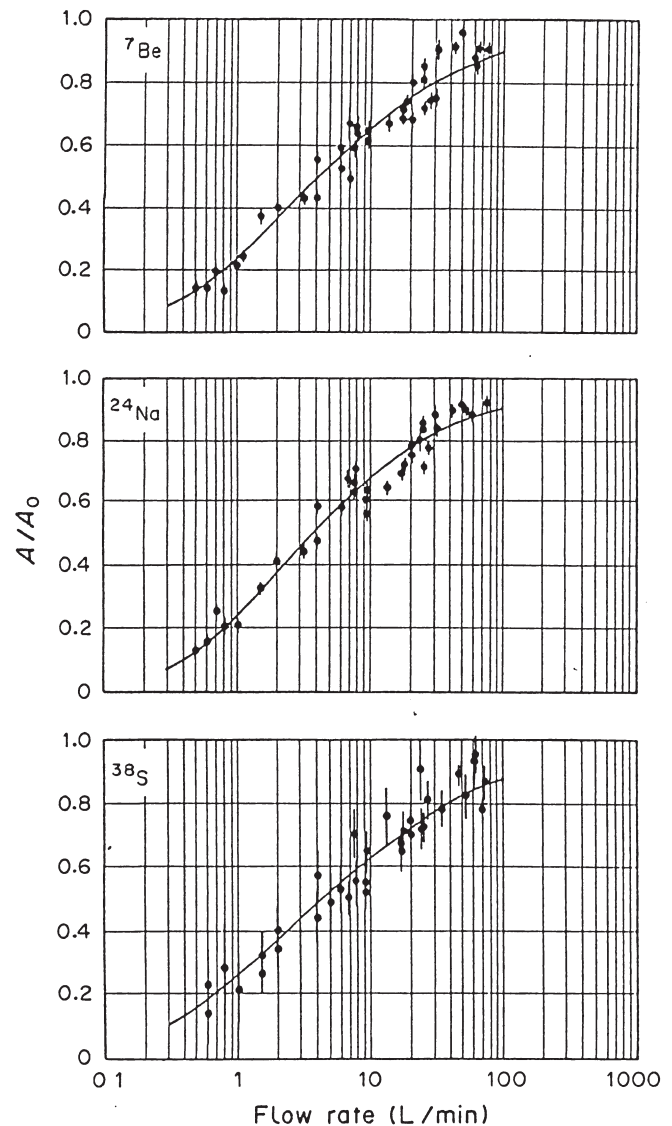


Figure 4. The relationship of  $A/A_0$  vs flow-rate for  $^7\text{Be}$ -,  $^{24}\text{Na}$ -, and  $^{38}\text{S}$ -aerosols.  $\bullet$ : experimental,  $-$ : calculated using SALS code.

(geometric mean radii) and  $\sigma_g$  (standard geometric deviation). They were determined to be  $r_g = 0.027 \pm 0.005 \mu\text{m}$  and  $\log \sigma_g = 0.36 \pm 0.02$  for  $^7\text{Be}$ ,  $r_g = 0.027 \pm 0.01 \mu\text{m}$  and  $\log \sigma_g = 0.44 \pm 0.04$  for  $^{38}\text{S}$ , and  $r_g = 0.028 \pm 0.009 \mu\text{m}$  and  $\log \sigma_g = 0.33 \pm 0.02$  for  $^{24}\text{Na}$ -aerosols. The obtained log-normal distributions are shown in Figure 5, together with that of the non-radioactive aerosols observed during the machine operation.

As Figure 5 shows, the particle size distributions for  $^7\text{Be}$ -,  $^{24}\text{Na}$ - and  $^{38}\text{S}$ -aerosols are very similar to each other, although the standard geometric deviations are slightly different. It is very interesting that these aerosols are of about the same radii regardless of the differences of the physical and chemical properties among them. This fact suggests that the aerosol formation of these nuclides proceeds via a simple physical adsorption to ambient non-radioactive aerosols.<sup>13</sup> The aerosol size distributions for other isotopes, such as iron, scandium, and manganese isotopes, were not determined because of their low radioactivities, though their size distributions are considered to be similar to those for  $^7\text{Be}$ ,  $^{24}\text{Na}$ , and  $^{38}\text{S}$ .

Naturally occurring radioactive aerosols of radon and/or thoron daughters also have a similar size distribution, but their geometric mean radii are considerably greater than the present values. It is also reported that the radioactive aerosols of fission products from atomic bomb tests have different size distributions in the stratosphere and troposphere, depending on the characteristics of the ambient non-radioactive aerosols.<sup>17</sup>

The size distribution of non-radioactive aerosols obtained in this experiment was of a log-normal shape with a geometric mean radius of  $0.01 \mu\text{m}$  and  $\log \sigma_g = 0.3$ , as shown in Figure 5, and the aerosol concentrations were  $(\sim 1.5\text{--}4.3) \times 10^5/\text{cm}^3$ , depending on the beam intensity. It is very interesting that the non-radioactive aerosols formed during machine operation were of sizes much smaller than those of the non-radioactive aerosols present in the natural environment. Most atmospheric aerosols in the submicron region are generally considered to contain sulfate formed through the photochemical oxidation of  $\text{SO}_2$ <sup>18</sup> of which the concentration in the atmospheric air is  $5\text{--}1.5 \mu\text{g}/\text{m}^3$ .<sup>19</sup> In this experiment, the air is exposed to very high radiation of about  $10^4 \text{ R/h}$  at the sampling inlet. Under these conditions, the non-radioactive submicron aerosols in the air of EP-2 tunnel are considered to be mostly sulfate aerosols formed through radiolytic oxidation reactions of  $\text{SO}_2$ . Indeed, it was confirmed by ion-chromatographic analysis that the non-radioactive aerosols in the size range below  $0.45 \mu\text{m}$  in diameter,

contained sulfate compounds in significant quantity.<sup>20</sup>

Therefore, it seems likely that the  $^7\text{Be}$ -,  $^{24}\text{Na}$ -, and  $^{38}\text{S}$ -aerosols are formed by the attachment of these nuclides to the non-radioactive aerosols containing  $\text{SO}_4^{2-}$ , which are formed by radiation-induced reactions. These radioactive aerosol size distributions ( $F(r)$ ) can be determined by multiplying the non-radioactive aerosol size distribution ( $N(r)$ ) by the attachment coefficient  $\beta(r)$ .  $\beta(r)$  was calculated using the following equation, assuming that these radioactive atoms are neutral and the attachment proceeds via simple physical adsorption:

$$\beta(r) = \frac{\pi r^2 \bar{v}}{\left(1 + \frac{\bar{v}r}{4D}\right)}, \quad (5)$$

where  $r$  is an aerosol radius,  $\bar{v}$  the average velocity and  $D$  the diffusion coefficient.  $D$  and  $\bar{v}$  are defined by the following equations:

$$D = \frac{3}{8} L \sqrt{\frac{\pi k T (m+M)}{mM}}, \quad (6)$$

$$\bar{v} = \sqrt{\frac{8kT}{\pi M}}, \quad (7)$$

where  $m$  and  $M$  are the mass of nuclide and air molecule, respectively,  $T$  the temperature (296 K),  $k$  Boltzmann's constant, and  $L$  the mean-free path. By using the thus-calculated  $\beta(r)$  for each nuclide, the radioactive size distribution ( $F(r)$ ) was obtained. As depicted in Figure 6, the thus-calculated distributions were almost the same as those for  $^7\text{Be}$ -,  $^{24}\text{Na}$ -, and  $^{38}\text{S}$ -aerosols. This is indicative that these aerosols are formed by a simple physical attachment to the ambient sulfate aerosols<sup>4</sup>.

In addition, the simple adsorption of the nuclide to the ambient aerosols was confirmed by the experiments using Ar gas containing DOP aerosols of a given poly-disperse size distribution,<sup>21,22</sup> and the sample gas was irradiated by well-collimated monoenergetic neutrons of 65 MeV, where no significant radiations without neutrons were concomitant. It was confirmed that  $^{38}\text{Cl}$ - and  $^{39}\text{Cl}$ -aerosols were formed only for the argon gas containing the DOP aerosols and were not observed without the DOP aerosols. Figure 7 shows the DOP size distribution and the activity-weighted size distribution. Here, the activity-weighted size distribution was obtained from the total activity of  $^{38}\text{Cl}$  and  $^{39}\text{Cl}$  to the end of sampling. The distribution curves were normalized to the respective maximum concentrations.

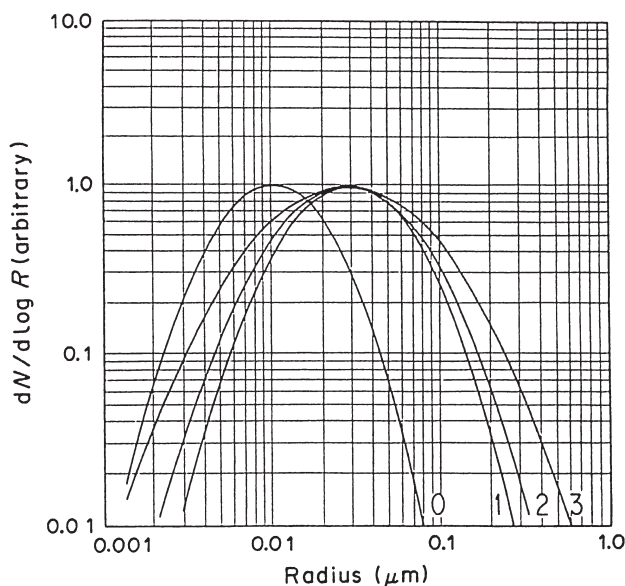


**Figure 5.** The log-normal distributions of  $^7\text{Be}$ -,  $^{24}\text{Na}$ -, and  $^{38}\text{S}$ -aerosols. 0: non-radioactive aerosol, 1:  $^{24}\text{Na}$ , 2:  $^7\text{Be}$ , 3:  $^{38}\text{S}$ .

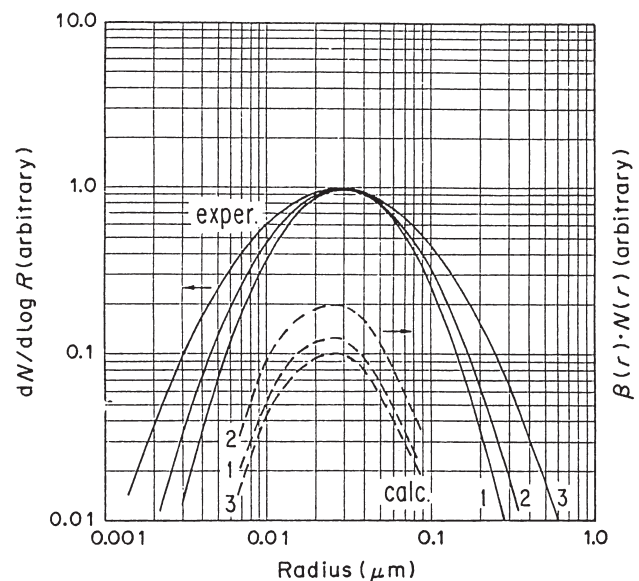


**Figure 6.** Comparison between the log-normal aerosol size distributions obtained experimentally and those calculated.

—: experimental, - - - -: calculated; 1:  $^{24}\text{Na}$ , 2:  $^7\text{Be}$ , 3:  $^{38}\text{S}$

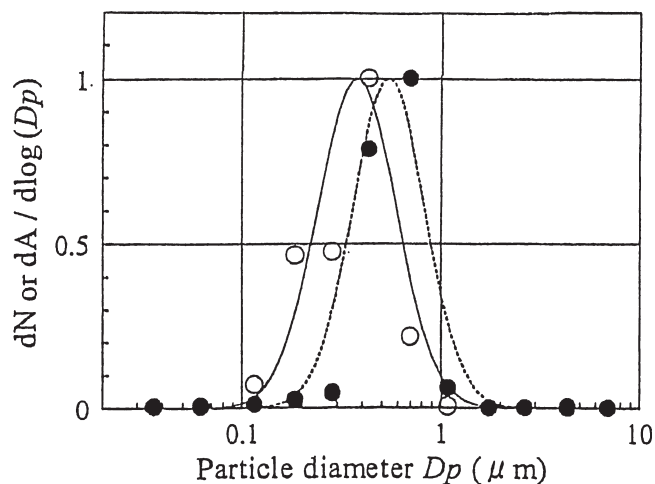
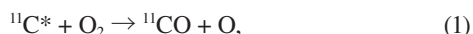


**Figure 7.** Size distribution of  $^{38}\text{Cl}$  and  $^{39}\text{Cl}$  attached DOP aerosols formed by the irradiation of 45 MeV neutrons  
○:measured number size distribution, ●:measured activity size distribution

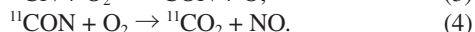
The activity-weighted size distribution curve slightly shifted toward larger particle diameter, compared to the DOP size distribution, and the computed distribution was well fitted to the one obtained experimentally. This result is similar to those for  $^7\text{Be}$ -,  $^{24}\text{Na}$ -, and  $^{38}\text{S}$ -aerosols, and supports the formation mechanism of aerosol formation mentioned above.

The radionuclides produced via nuclear reactions would have large kinetic energies and/or charges at their birth and interact with the surrounding as hot atoms. After completion of these hot atom reactions, most of them are likely to attach to the surrounding non-radioactive aerosols. The present results support that the radioactive aerosol formation proceeds by a simple physical attachment to the ambient non-radioactive aerosols with a certain distribution.

**(c) Chemical forms of gaseous  $^{11}\text{C}$  and  $^{13}\text{N}$  and their formation mechanisms.** Table 1 summarizes the chemical compositions of gaseous  $^{11}\text{C}$  and  $^{13}\text{N}$ .  $^{11}\text{C}$  and  $^{13}\text{N}$  atoms behave as hot atoms and react with the ambient molecules to lead to the formation of  $^{11}\text{C}$ - and  $^{13}\text{N}$ -labeled species. Wolf et al.<sup>23,24</sup> extensively studied the reaction products of energetic  $^{11}\text{C}$  atoms produced in  $\text{N}_2\text{-O}_2$  gases of various compositions using 3-GeV and 10-MeV protons. They found that the primary products are  $^{11}\text{CO}$  and  $^{11}\text{CO}_2$ , and they explained the formation of these products by the following hot  $^{11}\text{C}^*$  atom reactions, which leads  $^{11}\text{CO}$  and  $^{11}\text{CN}$ :



The reaction (1) is exothermic by -128 kcal/mol, while the reaction (2) is endothermic by 50 kcal/mol. Thus formed  $^{11}\text{CN}$  is instantaneously oxidized to  $^{11}\text{CO}_2$ .



They also estimated that the reactivity of energetic  $^{11}\text{C}$  atoms toward  $\text{O}_2$  is nine-times larger than that toward  $\text{N}_2$ . From the reactivities of  $^{11}\text{C}$  with  $\text{O}_2$  and  $\text{N}_2$ , and their contents in the air, the percentages of  $^{11}\text{CO}$  and  $^{11}\text{CO}_2$  as primary products were evaluated to be about 70% and 30%, respectively. The composition is close to those, as shown in Table 1, and the present result supports the idea that the  $^{11}\text{C}$  species are formed by the above mentioned hot atom reactions.

On the other hand, the major species for  $^{13}\text{N}$  were  $^{13}\text{N}_2$  and  $^{13}\text{NO}_2$ , and although smaller quantities of  $^{13}\text{NO}$  and  $\text{H}^{13}\text{NO}_2$  were also observed, significant quantities of  $\text{H}^{13}\text{NO}_3$  were not detected. The recoil  $^{13}\text{N}$  atoms would attack nitrogen molecules by hot-atom reactions, leading directly the  $^{13}\text{N}_2$  formation.

**Table 1: (a) Fractions of aerosol and gaseous components and (b) chemical species of gaseous components**

**(a) Fractions of aerosol and gaseous components**

Nuclide	Component	
	Aerosol Component	Gaseous Component
$^{11}\text{C}$	1.9 %	98.1 %
$^{13}\text{N}$	1.9 %*	98.1 %
$^{15}\text{O}$	0.5 %**	99.5 %
$^{18}\text{F}$	0.05 %**	99.95 %
$^{38}\text{Cl}^{***}$	73 %	27 %
$^{39}\text{Cl}^{***}$	72 %	28 %
$^{38}\text{S}^{***}$	50 %	50 %

\* :  $\pm 0.4\%$ , \*\* :  $\pm(0.02\sim 0.04)\%$ , \*\*\* : A NaOH loaded filter was used to collect gaseous components.

**(b) Chemical species**

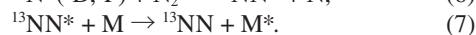
$^{11}\text{C}$  species

$^{11}\text{CO}$  : ~80%,  $^{11}\text{CO}_2$  : ~20%

$^{13}\text{N}$  species

$^{13}\text{N}_2$  : ~55%,  $^{13}\text{NO}_2$  : ~45%, others : less than 1%

It is also considered that a large fraction of the kinetically thermalized recoil  $^{13}\text{N}$  atoms would be electronically excited at the time of the reaction. The excited states are considered to be  $\text{N}(^2\text{D})$  and  $\text{N}(^2\text{P})$ , having excitation energies of 2.38 and 3.57 eV, respectively. Hence, the excited  $^{13}\text{N}^*$  atoms could supply the activation energy necessary for an exchange with nitrogen molecules<sup>25</sup>:



The kinetic data indicate that  $^{13}\text{NO}_2$  could be produced through a subsequent oxidation of  $^{13}\text{NO}$  with radiolytic products of  $\text{O}_3$ .  $^{13}\text{NO}$  is a primary product from hot and thermal reactions of recoil  $^{13}\text{N}$  atom with oxygen molecules;



The relative yields of  $^{13}\text{N}_2$  and  $^{13}\text{NO}_2$  suggest that the recoil  $^{13}\text{N}$  atoms are more likely to react faster with oxygen molecules by a factor of about 2.5 as compared with the reaction with nitrogen molecules.

The  $G$ -value for ozone formation in air was also calculated to be 6.4 (molecules/100 eV) at a dose rate of  $6 \times 10^{16} \text{ eV g}^{-1} \text{ s}^{-1}$ , which was slightly smaller than the value of 7.4 obtained by Willis et al.<sup>26</sup> at a high dose rate of  $10^{23} \text{ eV g}^{-1} \text{ s}^{-1}$ .

#### 4. Summary

The formation of radioactive aerosols was explained by a simple physical attachment of radioactive nuclides to ambient aerosols, and the size distributions of radioactive aerosols depended on the size distributions of ambient aerosols. It is considered that the non-radioactive aerosols of a submicron range contain sulfate formed by radiolytic reactions in the air of accelerator tunnels, where the air is exposed to very high radiations.

Most of  $^{11}\text{C}$  and  $^{13}\text{N}$  produced in the air are present in gaseous species, and are formed through hot-atom reactions and following thermal reactions. The chemical compositions of  $^{11}\text{C}$  and  $^{13}\text{N}$  were extensively studied. The results can be used for quantitative evaluations of the internal doses.

## References

- (1) *Accelerator Technical Design Report for J-PARC*, Ed. Accelerator Group, JAERI/KEK Joint Project Team, KEK Report 2002-13(2003).
- (2) K. Kondo, H. Muramatsu, and Y. Kanda, *Int. J. Appl. Radiat. Isot.* **35**, 939 (1984).
- (3) H. Muramatsu, K. Kondo, Y. Kanda, and S. Takahara, *Proc. 5th Symp. Aerosol Sci. Tech. Tsukuba*, Japan, 1984, p 375.
- (4) H. Muramatsu, K. Kondo, Y. Kanda, and S. Takahara, *Appl. Radiat. Isot.* **39**, 413 (1986).
- (5) T. Miura, Y. Oki, Y. Kanda, and K. Kondo, *Proc. Advanced Nuclear Energy Research –Near Future Chemistry in Nuclear Energy Field*, Oarai, Ibaraki, Japan, 1989, p 100.
- (6) J. B. Cumming, V. Agoritas, and R. Witkovar, *Nucl. Instrum. Methods* **180**, 37 (1981).
- (7) N. A. Fuchs, I. B. Stechikina, and V. I. Starosselskii, *J. Appl. Phys.* **13**, 280 (1962).
- (8) The SALS program (statistical analysis with least-square fitting) was developed by T. Nakagawa and Y. Oyanagi, the University of Tokyo.
- (9) A. Endo, Y. Oki, Y. Kanda, T. Oishi, and K. Kondo, *Radiat. Prot. Dosim.* **93**, 223 (2001).
- (10) Y. Kanda, Y. Oki, A. Endo, M. Numajiri, and K. Kondo, *J. Radioanal. Nucl. Chem.* **247**, 25 (2001).
- (11) Y. Kanda, T. Momose, and M. Taira, *Radiat. Phys. Chem.* **48**, 49 (1996).
- (12) Y. Kanda, T. Miura, and H. Nakajima, *Radiat. Phys. Chem.* **73**, 213 (2005).
- (13) L. Lassen and G. Z. Rau, *Z. Phys.* **160**, 504 (1960).
- (14) M. Shimo, T. Torii, and Y. Ikebe, *J. At. Energy Soc. Jpn.* **23**, 59(1981).
- (15) S. Nakatani, *J. Meteorol. Soc. Jpn.* **50**, 408 (1972).
- (16) *Air Chemistry and Radioactivity*, Ed. C. E. Junge, Academic Press, New York, 1976, p 224.
- (17) M. I. Kollstein, P. I. Drevingky, E. A. Martell, C. W. Chagon, J. E. Manson, and C. E. Junge, Progress Report II, GRD Research Notes, No.24, 1 (1959).
- (18) *Air Chemistry and Radioactivity*, Ed. C. E. Junge, Academic Press, New York, 1976, p 153.
- (19) M. H. Marlow and R. L. Tanner, *Anal. Chem.* **48**, 1999 (1976).
- (20) Y. Kanda, private communication.
- (21) A. Endo, H. Noguchi, Su. Tanaka, Y. Kanda, Y. Oki, T. Iida, K. Sato, and S. Tuda, *Appl. Radiat. Isot.* **56**, 615 (2002).
- (22) K. Sato, S. Yokoyama, H. Noguchi, Su. Tanaka, T. Iida, S. Furuichi, Y. Kanda, and Y. Oki, *J. Nucl. Sci. Tech. Suppl.* **4**, 518 (2004).
- (23) R. A. Ferrieri and A. P. Wolf, *Radiochim. Acta* **34**, 69 (1983).
- (24) H. J. Ache and A. P. Wolf, *J. Phys. Chem.* **72**, 1988 (1968).
- (25) C. Willis, A. W. Boyd, and M. S. Young, *Can. J. Chem.* **48**, 1515 (1970).